– Report –

A monthly mean dataset of global oceanic temperature and salinity derived from Argo float observations

Shigeki Hosoda[1]*, Tsuyoshi Ohira[2], and Tomoaki Nakamura[1]

We produced a global monthly dataset of temperature and salinity using data from Argo floats, Triangle Trans-Ocean Buoy Network (TRITON), and available conductivity-temperature-depth (CTD) casts. The Argo project started from 2000, and the number of floats is increasing yearly throughout the global ocean. The Argo floats observe pressure, temperature and salinity from the sea surface down to 2000 dbar and enable the production of monthly global datasets of temperature and salinity. We have created Grid Point Value of the Monthly Objective Analysis using Argo float data (MOAA GPV) that contains optimally interpolated temperature and salinity values at selected standard pressure levels on a 1° grid in the global ocean. The dataset is freely available on the Argo website of the Japan Agency for Marine-Earth Science and Technology (JAMSTEC) at http://www.jamstec.go.jp/ARGO/J_ARGOe.html.

Keywords : Argo float, monthly mean dataset, objective analysis, global distribution, TRITON buoy

Corresponding author:
    Shigeki Hosoda
    Japan Agency for Marine-Earth Science and Technology (JAMSTEC)
    2-15, Natsushima, Yokosuka, Kanagawa, 237-0061, Japan
    +81-46-867-9456
    hosodas@jamstec.go.jp

1. Introduction

A global observational dataset of temperature and salinity is necessary for both general monitoring of the world ocean and providing information on climate change. Previous datasets routinely contained subsurface temperatures only. For example, White (1995) constructed a monthly mean temperature dataset from the surface to subsurface using observations from limited expendable bathythermograph (XBT) and hydrographic stations. The statistical parameters of long-term and basin-wide temperature variation were used to create global temperature maps. Even though the dataset has been extremely useful for oceanographers, it has disadvantages. The maximum depth in the dataset is shallow (400 m), and the horizontal resolution is relatively coarse (2.5˚ × 5˚). Hence it cannot be used to investigate the detailed structure of temperature variations below the thermocline.

In addition, there were no global high-resolution salinity datasets because of the insufficient number of available salinity profiles. Observational salinity datasets, which could aid in the study of ocean circulation and climate change mechanisms, would benefit many researchers.

The Argo project, which began in 2,000, involves the deployment of profiling floats to monitor temperature and salinity automatically in 10-day intervals down to a depth of 2,000 dbar (Argo Science Team, 2001). The target spatial density for the Argo float array is one float per 3˚ square in the world ocean. In late October 2007 the number of observing floats reached 3,000, providing complete coverage of the world ocean for the first time. Therefore, we have begun to construct a gridded monthly mean dataset of global temperature and salinity.

We used the optimal interpolation (OI) method to construct a gridded dataset without some marginal seas (Gandin, 1963; Mizuno, 1995). This simple method is frequently used to estimate grid-point values from observational data. Its major benefit is that it allows estimation of errors which cannot be obtained by simple averaging. To apply the OI, two statistical parameters from historical observed data are needed a priori: the spatial decorrelation radius and the error information (signal-to-noise ratio). Some important studies have discussed the spatial distribution of these parameters for the ocean's temperature field. For example, Meyers et al. (1991) showed the decorrelation radius and RMS signal-to-noise ratio of the sea surface temperature and depth of the 20˚C isotherm in the tropical Pacific, using XBT observations and some ship-recorded data. White

(1995) produced global maps of decorrelation radius and error information using subsurface historical temperature data. We applied the values published in the latter study, because their analysis covered the world ocean.

To estimate salinity, decorrelation radius and error information on salinity should be used. However, there are no such statistical parameters because long-term historical salinity data are still too sparse. Therefore, we adopted decorrelation radius and error information on temperature to produce the salinity field.

In this paper, we describe data and methods of our analysis given in Table 1. The name of the dataset is Grid Point Values of the Monthly Objective Analysis using the Argo data (MOAA GPV; Hosoda and Minato, 2003; Hosoda et al., 2006), which is available for access on our website.

2. Data and method
2.1. Data

We used profile data from the Argo floats array, Triangle Trans-Ocean Buoy Network (TRITON), and available conductivity-temperature-depth profilers (CTD) onboard research vessels. The reason for using the CTD data is that collected data of the Argo floats and the TRITON buoys did not cover the whole ocean uniformly for several years after the initial deployment of Argo floats. In the following subsections, each data type is described in more detail.

2.1.1. Argo float data

Real-time quality-controlled (rQC) data are available. The rQC is conducted automatically on the Argo float data and transmitted within 24 hours after observation (Argo Science Team, 2000). Also, delayed-mode quality controlled (dQC) data, which make use of scientific knowledge, are applied to the Argo float data within six months (Argo Data Management Team, 2002; Wong et al., 2003; Wong and King, 2005). We used rQC data (and also dQC data for re-analysis) a via the FTP site of the Argo Global Data Assembly Center (GDAC). The accuracies of the temperature, salinity, and pressure sensors on the Argo floats are ±0.005˚C, ±0.01 psu, and ±5 dbar respectively (Argo Science Team, 2000).

2.1.2. TRITON buoy data

We used rQC data of the TRITON buoys, which are deployed in the western tropical Pacific Ocean. These hourly data were obtained from the TRITON Data

Management System (TDMS; Ueki et al., 2002). We collected these data because both temperature and salinity are included in the profiles. The accuracies of ±0.002˚C for temperature and ±0.02 psu for salinity are conserved by checking the sensor once a year; the accuracy is equivalent to the Argo float data. From the hourly data, we calculated the averaged monthly values at each buoy from the hourly data.

2.1.3. CTD cast data

The available CTD data were obtained from ships of the Japan Meteorological Agency (JMA), the Japan Coast Guard (JCG), the Japan Fishery Agency (JFA), the Fisheries Research Agency (FRA), and the Japan Agency for Marine-Earth Science and Technology (JAMSTEC). Quality checks of these data were already conducted, and the accuracies of the data are equivalent to or higher than those of the Argo float data. Though the number of CTD data used is limited, we will collect more CTD data from other countries, ships, and databases to produce more accurate maps.

2.2. Data check

We collected the profiles of temperature and salinity that met the conditions in Table 2. Data selection was necessary to allow vertical interpolation of the profiles and to avoid inconsistency of vertical profiles at each grid point. In our analysis, we used no-error data ("good" flag data) to avoid the possibility of producing large-error maps. Further, to avoid producing large-error interpolated data, we removed profiles with too large a spacing of observed levels. The TRITON buoy data were not checked because their profiles were shorter and more discrete.

2.3. Data processing
2.3.1. Vertical coordinate transformation

We calculated temperature and salinity on each pressure surface because the vertical coordinate in most profiles is defined by pressure, except for those of the TRITON buoys and the *World Ocean Atlas 2001* (WOA01; Boyer et al., 2002; Stephens et al., 2002). In this subsection, we showed how to transform a depth vertical coordinate to a pressure one. *z*, *p*, and *g* are defined as depth, pressure, and gravitational acceleration respectively, and downward is defined to be positive. The relationship between pressure and depth is described by the hydrostatic balance equation (e.g. Gill, 1982),

$$dp = \rho g dz, \tag{1}$$

where ρ is the in situ density, which we calculated from pressure, temperature, and salinity. From Eq. (1), the pressure at depth Z is written by,

$$p = \int_0^Z \rho g dz. \tag{2}$$

To apply Eq. (2) for each profile in depth vertical coordinates, we obtained profiles in pressure vertical coordinates.

2.3.2. Vertical interpolation and extrapolation

The selected profiles were used for the OI after interpolation onto a standard pressure grid using the Akima spline (Akima, 1970). For all interpolated profiles, we checked again vertical density stability and removed the data with density inversion. When the deepest level of Argo profile was between 1,950 and 2,000 dbar, we calculated the values at 2,000 dbar through extrapolation, because some of the Argo floats did not observe at 2,000 dbar due to their float settings. This method of extrapolation worked well because at around 2,000 dbar the change in vertical profile gradients was so small that the artificial error was smaller than the original accuracies of temperature and salinity data.

2.3.3. Statistical checks using climatological standard deviation

To remove profiles with large errors from collected data, we performed statistical checks using monthly mean climatology and annual mean standard deviation from the WOA01. When the difference from temperature and salinity climatology was over three times as large as the standard deviation at a given level, the data at the level were removed. In some area with large variability, there is a possibility of removing "correct data" by this method. However, we confirmed that such correct data were not removed, at least in the analyzed period. The percentage of removed data per month was about 3% of the total.

2.4. OI method

We used the following OI method. Take *T* to be an arbitrary quantity that has been observed for a long time and has known statistical values. The observed value at a point is described as $T_0(j)$:

$$T_o(j) = T_t(j) + \varepsilon(j). \tag{3}$$

Here, $T_i(j)$ is a true value at a point *j*, and $\varepsilon(j)$ is white noise

caused by internal waves, internal tides, and mesoscale eddy activity. Since the noise is independent of signals, ensembles mean of the product of ε by T_0 or T_i are described as,

$$< (T_o - T_c)\,\varepsilon \, >= 0$$
$$< (T_t - T_c)\,\varepsilon \, >= 0\,, \tag{4}$$

where T_c is a first-guess value that was obtained from the monthly mean climatology in the upper 1,500 dbar (from the seasonal mean climatology in 1,500-2,000 dbar) of the WOA01. Ensemble mean of the product of noise is also written by,

$$< \varepsilon(m)\varepsilon(n) > = \begin{cases} 0 & \cdots \quad (m \neq n) \\ \sigma_e & \cdots \quad (m = n) \end{cases}, \tag{5}$$

where m and n are observation and estimation points respectively. σ_e is noise variances obtained from error information (see section 2.5). An estimation value and an estimation error are described as T_a and e_a, and the relation between the two values at a point are written using the J observed data points of T_0,

$$T_a(i) - T_c(i) = \sum_{j=1}^{J} w(j\,;i)\{T_o(j) - T_c(j)\}\,, \tag{6}$$

and

$$e_a(i) = T_a(i) - T_t(i). \tag{7}$$

Here, w is a weight function for each observed value.

   If an ensemble mean of the estimation error E^2 is calculated from e_a using Eqs. (3)-(7),

$$E^2(i) = < e_a^{\,2}(i) >$$
$$= < \{T_t(i) - T_c(i)\}^2 > -2\sum_{j=1}^{J} w(j;i) < \{T_t(i) - T_c(i)\}\{T_t(j) - T_c(j)\} >$$
$$+ \sum_{j=1}^{J}\sum_{k=1}^{J} w(j;i)w(k;i) < \{T_t(j) - T_c(j)\}\{T_t(k) - T_c(k)\} >$$
$$+ \sum_{j=1}^{J} w(j;i)^2 \sigma_e(j). \tag{8}$$

To minimize the estimation error, Eq. (8) satisfies the following relation for each j:

$$\frac{\partial\{E^2(i)\}}{\partial w(j;i)} = -2 < \{T_t(i) - T_c(i)\}\{T_t(j) - T_c(j)\} >$$
$$+ 2\sum_{k=1}^{J} w(k;j) < \{T_t(j) - T_c(j)\}\{T_t(k) - T_c(k)\} > + 2w(j;i)\sigma_e(j) = 0. \tag{9}$$

Using Eq.(9), Eq.(8) at point i is written as follows:

$$\sum_{k=1}^{J}\Big[< \{T_t(j) - T_c(j)\}\{T_t(k) - T_c(k)\} > +\delta_{jk}\sigma_e(j) \Big] w(k;i)$$
$$= < \{T_t(i) - T_c(i)\}\{T_t(j) - T_c(j)\} >, \tag{10}$$

where δ_{jk} is a Kronecker delta described by,

$$\delta_{jk} = \begin{cases} 1 & \cdots \quad (j = k) \\ 0 & \cdots \quad (j \neq k) \end{cases}. \tag{11}$$

Rewriting Eq. (10) in matrix notation, the weight function is defined as

$$W = A^{-1}B\,. \tag{12}$$

Here W is a matrix of the weight function described by $W(j\,;i) = w(j\,;i)$, A is a matrix of covariance, defined between observation points at m and n as,

$$A(j,k) = < \{(T_t(j) - T_c(j)\}\{T_t(k) - T_c(k)\} > +\delta_{jk}\sigma_e(j), \tag{13}$$

with B taking a similar form,

$$B(j,i) = < \{T_t(i) - T_c(i)\}\{T_t(j) - T_c(j)\} >. \tag{14}$$

The elements of these covariance matrices are calculated using σ_e, and σ_c which is a signal variance obtained from annual mean standard deviation in the WOA01,

$$A(j,k) = \begin{cases} \sigma_c(j)e^{-\{dx_1(j,k)/D_x + dy_1(j,k)/D_y\}} & \cdots \quad (j \neq k) \\ \sigma_c(j) + \sigma_e(j) & \cdots \quad (j = k) \end{cases}, \tag{15}$$

$$B(j,i) = \sigma_c(j)e^{-\{dx_2(j,i)/D_x + dy_2(j,i)/D_y\}}. \tag{16}$$

Here, dx_1 (dy_1) and dx_2 (dy_2) are defined as the zonal (meridional) distances between the observation points (dx_1 and dy_1) and observation and estimation points (dx_2 and dy_2), respectively. The zonal (meridional) e-folding scale D_x (D_y) in Eqs. (15) and (16) is given by the decorrelation radii in functions of depth and latitude a priori (see section 2.5). Thus, the weight function can be decided, and the estimation error for an arbitrary estimation value at point i, $T_a(i)$, is calculated from Eqs. (8) and (10),

$$E^2(i) = < \{T_t(i) - T_c(i)\}^2 > - \sum_{j=1}^{J} w(j;i) < \{T_t(i) - T_c(i)\}\{T_t(j) - T_c(j)\} >. \tag{17}$$

If the signal is constantly uniform in the analyzed area, Eq. (17) is rewritten simply,

$$E^2(i) = \sigma_c(i)\left\{ 1 - \sum_{j=1}^{J} w(j;i)e^{-\{dx_1(j,k)/D_x + dy_1(j,k)/D_y\}} \right\}. \tag{18}$$

Table 1. Summary of MOAA GPV

Method	2-dimensional optimal interpolation on pressure surfaces
Parameters	Temperature and salinity
Areas	Global Ocean: Pacific 60.5°N.-60.5°S., Atlantic 70.5°N.-60.5°S., Indian 30.5°N.-60.5°S. (Including the Bering Sea and excluding marginal seas)
Resolution	Horizontal: 1°×1°, 25 levels from 10 - 2,000dbar (Standard pressure levels: 10, 20, 30, 50, 75, 100, 125, 150, 200, 250, 300, 400, 500, 600, 700, 800, 900, 1,000, 1,100, 1,200, 1,300, 1,400, 1,500, 1,750, 2,000 dbar)
Data Source	Argo floats, TRITON buoys, available CTD casts
Period	From January 2001; ongoing

Table 2. Conditions of profile selection

Maximum depth	Deeper than 900 dbar
Minimum depth	Shallower than 15 dbar
Number of observed levels	More than 15 levels
Spacing of observed levels	< 400 dbar: less than 50 dbar, 400 - 1,000 dbar: less than 100 dbar > 1,000 dbar: less than 300 dbar

Table 3. Zonal and meridional decorrelation radii and noise-to-signal ratios

	Pacific			Atlantic			Indian		
0m	Zonal	Merid.	N/S	Zonal	Merid.	N/S	Zonal	Merid.	N/S
50°N	15.9	8.8	1.0	12.8	7.5	1.1	-	-	-
40°N	10.4	6.6	1.0	10.6	6.7	1.0	-	-	-
30°N	11.4	8.6	1.0	7.3	7.4	0.9	-	-	-
20°N	19.7	8.3	1.0	12.3	6.0	1.0	10.1	3.6	1.1
10°N	24.0	11.5	0.9	13.7	4.7	1.1	12.7	4.0	1.0
EQ	22.6	11.3	0.8	17.3	7.2	1.2	10.5	3.2	1.1
10°S	15.2	7.8	0.9	12.0	6.1	1.0	12.0	5.9	1.3
20°S	13.1	6.3	1.1	-	-	-	13.6	7.2	1.1
30°S	15.1	8.1	1.3	-	-	-	15.3	7.7	1.0
200m	Zonal	Merid.	N/S	Zonal	Merid.	N/S	Zonal	Merid.	N/S
50°N	8.9	5.9	1.3	5.9	2.6	1.1	-	-	-
40°N	10.6	5.4	1.3	7.3	2.5	1.1	-	-	-
30°N	17.6	4.0	1.2	7.9	4.1	1.1	-	-	-
20°N	21.3	6.0	1.1	7.3	3.3	1.2	20.2	11.3	1.6
10°N	19.2	7.4	1.1	4.9	5.4	1.2	12.9	5.7	1.2
EQ	12.5	7.0	1.0	5.3	3.4	1.1	7.1	4.9	1.1
10°S	13.0	4.8	1.0	7.7	2.4	1.0	5.4	7.4	1.1
20°S	9.4	6.2	1.2	-	-	-	16.7	7.0	1.1
30°S	10.8	6.9	1.5	-	-	-	18.5	6.5	0.9
400m	Zonal	Merid.	N/S	Zonal	Merid.	N/S	Zonal	Merid.	N/S
50°N	10.6	6.6	1.4	6.1	5.7	0.9	-	-	-
40°N	11.1	5.9	1.2	5.5	4.0	1.0	-	-	-
30°N	12.8	3.6	1.1	9.0	2.6	1.0	-	-	-
20°N	16.8	5.8	1.0	7.0	4.1	1.0	3.1	6.4	1.6
10°N	15.3	5.4	1.2	4.4	5.9	1.1	6.3	4.7	1.2
EQ	14.3	4.5	1.2	5.0	4.6	1.2	4.4	3.4	1.1
10°S	13.3	4.3	1.1	5.9	3.5	1.1	6.0	5.2	1.1
20°S	11.6	4.1	1.1	-	-	-	8.2	6.0	1.1
30°S	14.3	6.6	1.3	-	-	-	15.7	4.5	0.9

2.5. Decorrelation radius and error information

We used the decorrelation radius and error information values (signal-to-noise ratio) of White (1995) (Table 3). The values were given at a few levels (0, 200, and 400 m) for the temperature field. To define the values for all grids from surface to mid-depth, we linearly interpolated from 0 to 400 m and assumed constant values below 400 m. As there were no values recorded for salinity, we took these values to be the same as those for temperature. All values are given as a function of depth. We converted them to pressure coordinates using the method described in subsection 2.3.1.

2.6. Calculation of covariance matrices

For calculating the OI on a computer, if the matrices are too large, the computer memory requirements of the OI calculation are too heavy, and the calculation time is too long. Therefore, we limited the area of collected data in 20°(meridional) × 40° (zonal) boxes for each grid. If the number of data points in a given box was over 100, we simply chose the 100 nearest points.

2.7. Marginal seas and topography

The distribution of gridded bottom and coastal topography was the same as in the WOA01. However, some marginal seas (e.g. Mediterranean, Japan/East, Okhotsk) were removed from the OI regions. The Bering Sea data were kept in this analysis. If observed points located out of ocean grids of the OI, we excluded the data from the calculation.

3. Distribution of observed points and interpolation error

Fig. 1 shows a time series of the number of observed points at the two levels. At 10 dbar, the number of observed points is insufficient, and large spatial biases exist from 2001 to 2003 (Fig. 1a). Before 2004, the rate of increase is not uniform due to noncontinuous changes in the number of CTD observations. The number of observations at 2,000 dbar is approximately half of that at 10 dbar (Fig. 1b), because some floats are observed in the upper 1,500 dbar or shallower. In the global ocean, about a half of floats are observed in the Pacific Ocean (Fig. 1b-d). Increase rates are positive in all basins, but have recently been small in the Atlantic

and Indian Oceans.

Fig. 2 shows the spatial distribution of observed points from January 2001 to July 2007. In the North Atlantic and North Pacific oceans, a large increase occurred earlier, and the basins are almost covered after 2003. The entire Indian Ocean is almost covered by around 2003. Although the deployment of floats in the South Pacific Ocean is slower than that in other oceans, the South Pacific area is almost covered by 2004. In the western tropical Pacific, the TRITON buoy array effectively helps to cover the area. However, there is not complete coverage at 2,000 dbar until 2007, mainly because some floats observe upper 1,500 dbar or less due to technical reasons, especially in the tropical region. Finally, the Atlantic Ocean is almost filled with observations at 10 dbar by 2003, but the spatial density of the data is still small.

Fig. 3 provides maps of the ratio of estimated error to standard deviation (error ratio). These maps effectively show the data coverage, with smaller values implying a smaller error. At 10 dbar in the North Pacific, the error ratio is small (below 0.5) after July 2003 (Fig. 3a). The error ratio becomes small (below 0.5) in the South Pacific and Indian oceans after 2006. The error ratio in the Atlantic Ocean is larger than the other basins, reaching 0.5 in some regions due to the low spatial density of the observations. At 2000 dbar, the error ratio is still large (above 0.5) in most regions due to the lack of data even in 2007 (Fig. 3b).

4. Summary and discussion

We produced a global 1°grid dataset (MOAA GPV) of monthly temperature and salinity distributions using two-dimensional OI on pressure levels from the surface to 2000 dbar. It is the first time such monthly global maps of oceanic temperature and salinity datasets have been produced routinely. The data were estimated from Argo floats, TRITON buoys, and CTD cast observations. This paper has described the dataset and OI method in detail, as well as the distributions of observed points used for the monthly maps and error ratios.

From the monthly maps and the dataset of temperature and salinity, we are producing maps of potential density, sea-level height, and geostrophic current velocities based on the 2000-dbar data. Furthermore, we are displaying three-dimensional maps of temperature, salinity, and other quantities in our web gallery. All
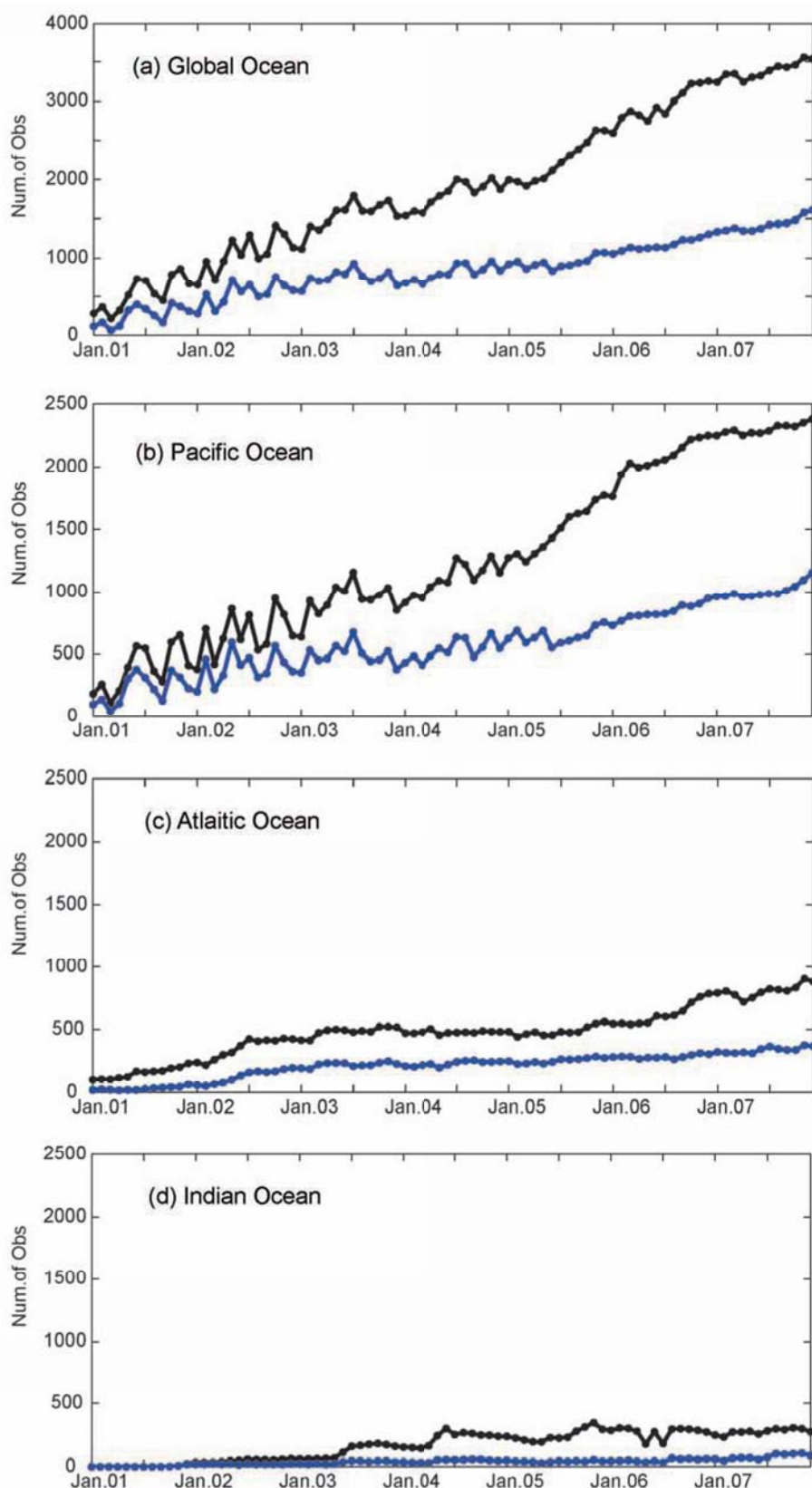
Figure 1. Number of observations used for the monthly maps of temperature and salinity in the global ocean (a), the Pacific Ocean (b), the Atlantic Ocean (c) and the Indian Ocean (d). Black (blue) line shows the time series at 10 dbar (2,000 dbar).
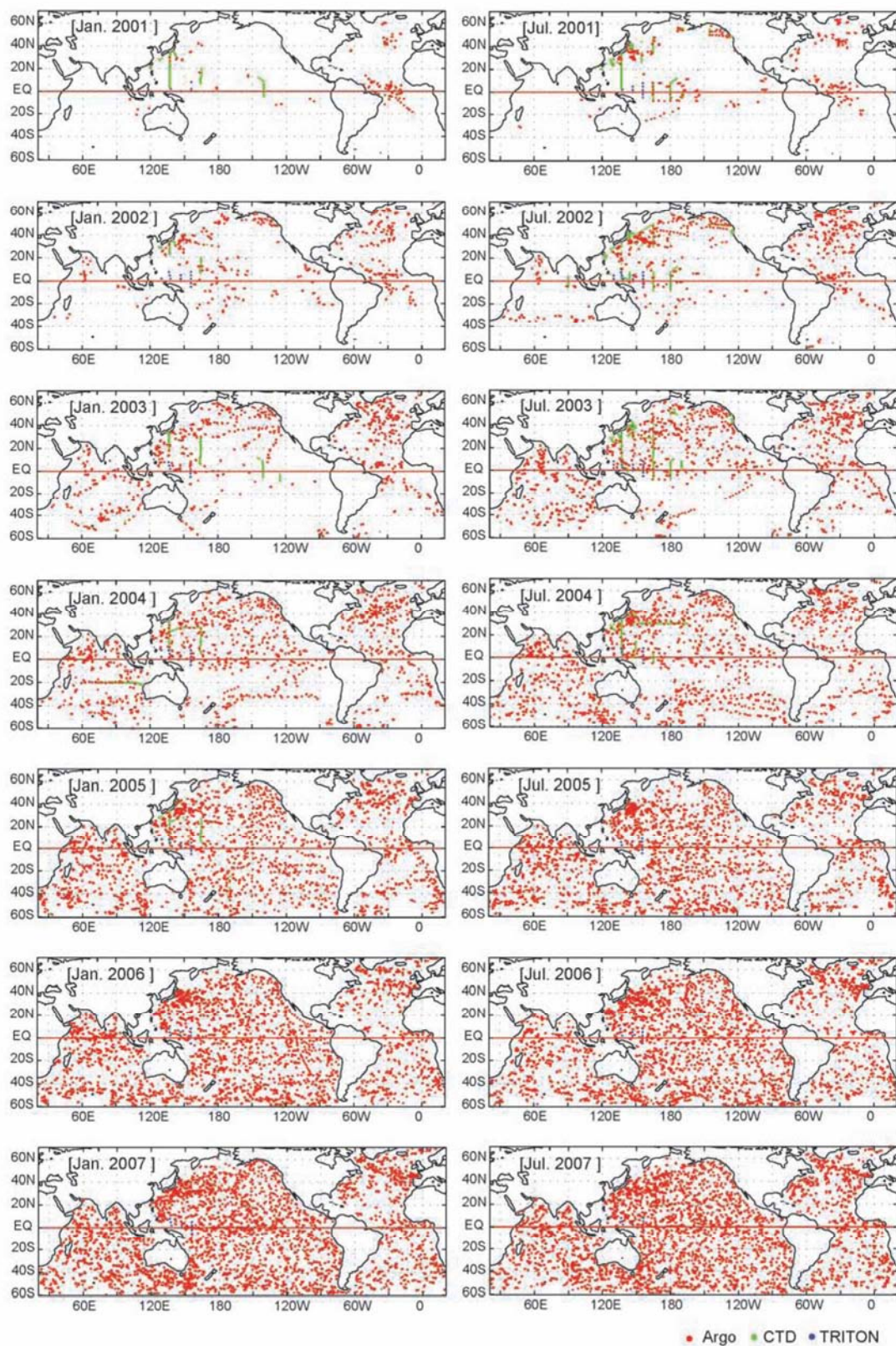
Fig. 2 (a)

Figure 2. Monthly maps of observed points used for the OI from January 2001 to July 2007. Levels of the maps are (a) 10 dbar and (b) 2,000 dbar. Red, green and blue dots show positions of the Argo floats, CTD casts and TRITON buoys respectively.
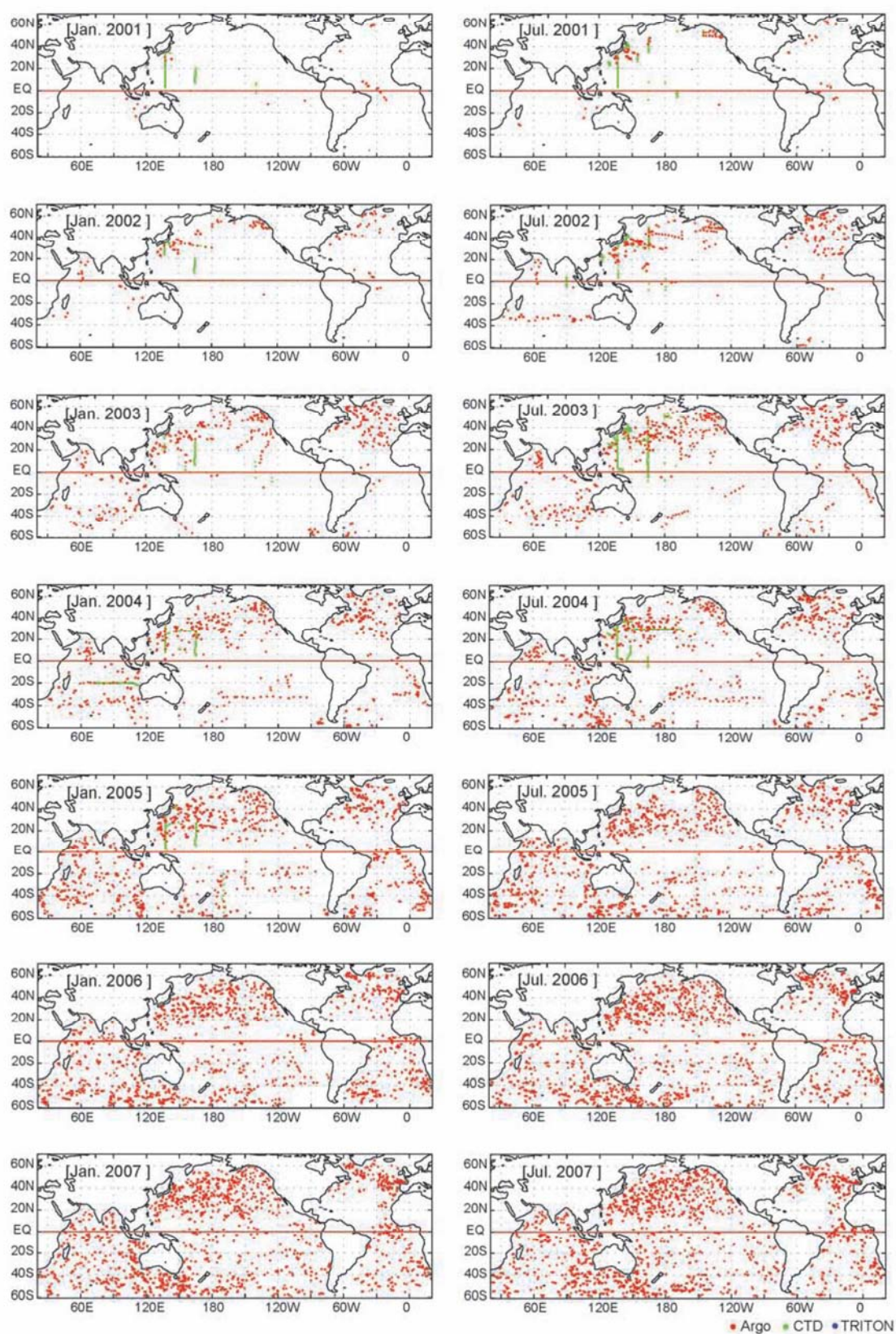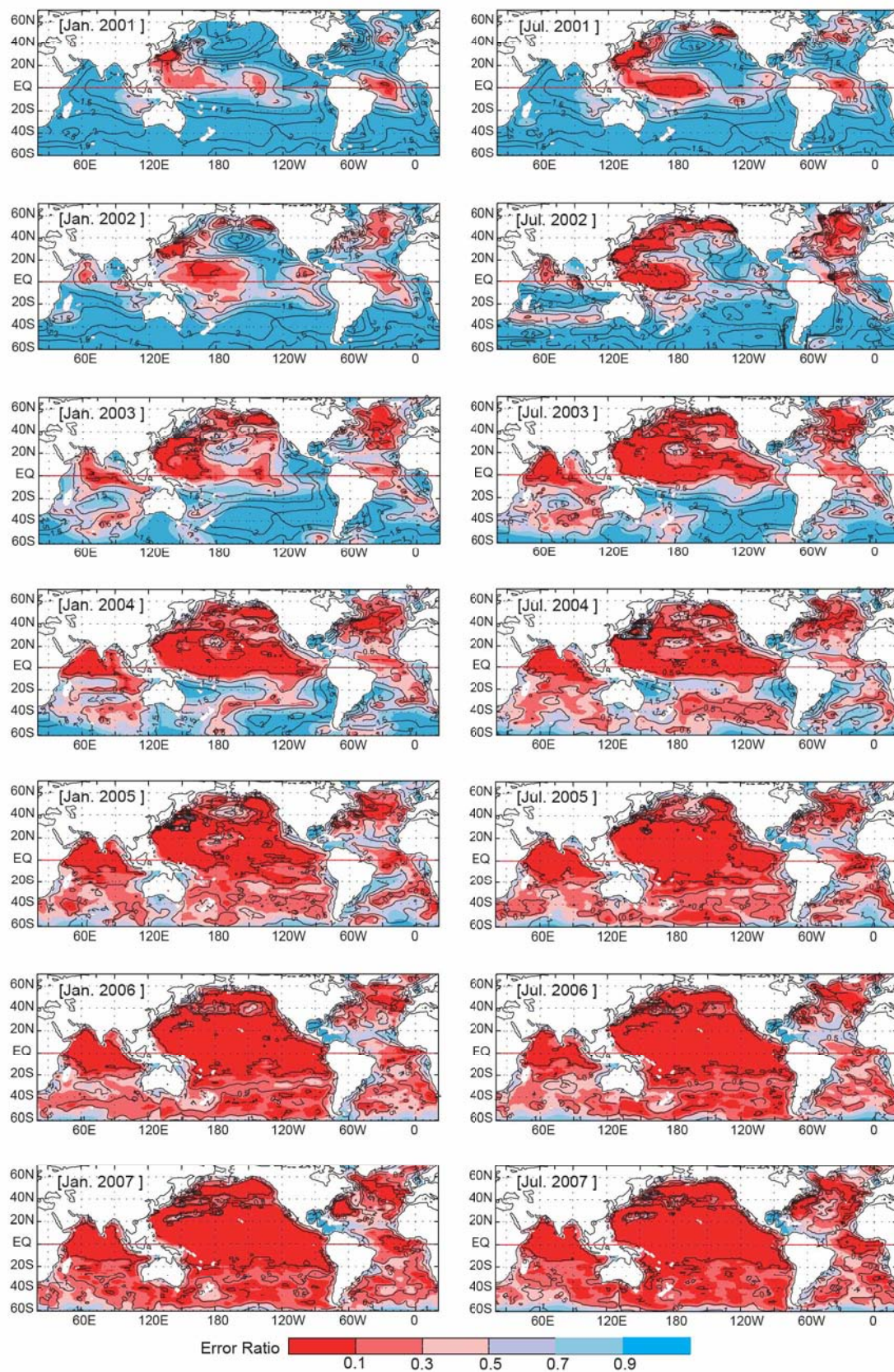
Fig. 2 (b)

Fig. 3 (a)

Figure 3. Monthly maps of the temperature interpolation error (contour) and its error ratio (color) from January 2001 to July 2007. Levels of the maps are (a) 10dbar and (b) 2,000dbar.
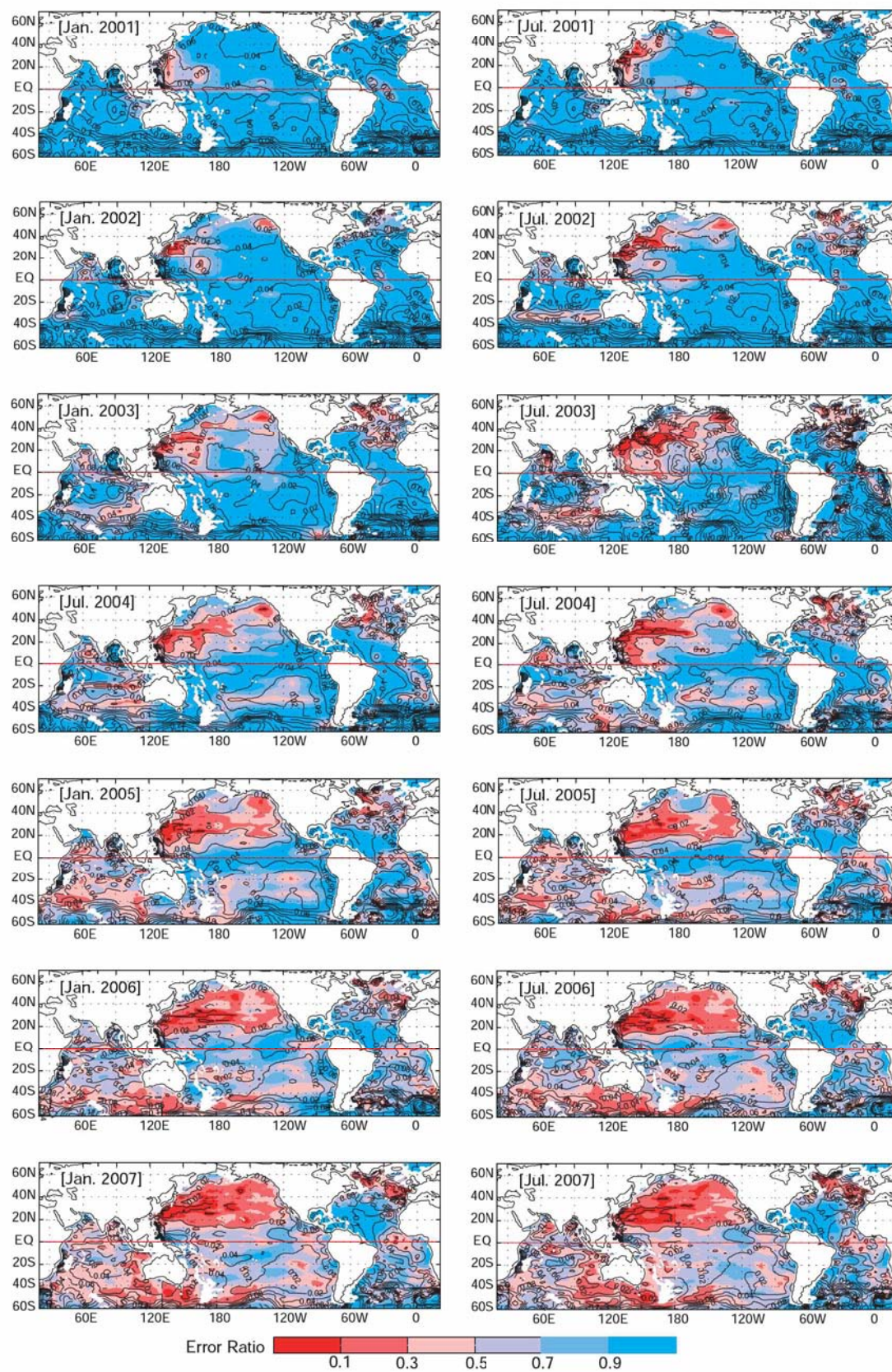
Fig. 3 (b)

datasets and maps are available from our website at http://www.jamstec.go.jp/ARGO/J_ARGOe.html.

Although global maps of temperature and salinity can be produced routinely due to the increase of float data, there are still large errors in some regions, particularly at western boundaries and in the deep ocean. Hence accurate estimation of important factors associated with global climate change, such as heat and freshwater transport, is still difficult. More data are needed to avoid these problems and produce datasets that have high accuracy everywhere.

In this analysis, we used the monthly or seasonal climatology and the annual standard deviation in the WOA01 for the first guess of the OI. This worked well for global mapping. However, in both the climatology and the standard deviation dataset, there are still some spatial and temporal biases in the distribution of historical observed points (Boyer et al., 2002; Stephens et al., 2002). Therefore, some spatial biases may be included in the first-guess data, and the biases may influence the accuracy of our estimated temperature and salinity. In the future, Argo data will have accumulated over a longer period, and we will be able to derive the climatology directly from the Argo data without spatial and temporal biases. Furthermore, we used the decorrelation radius and error information of temperature to derive the salinity fields. As future research, we also plan to estimate these values using the Argo data.

Acknowledgments

References

Akima, H. (1970), A new method for interpolation and smooth curve fittingbased on local procedures, *J. Assoc. Comput. Mech., 17*, 589-602.

Argo Data Management Team (2002), Report of the Argo Data Management Meeting. *Proc. Argo Data Management Third Meeting*, Marine Environmental Data, Ottawa, 42 pp.

Argo Science Team (2000), Report of the Argo Science Team Second Meeting. *Proc. Argo Science Team Second Meeting*, Southampton Oceanography Centre, Southampton, U.K., 35 pp.

Argo Science Team (2001), Argo: The global array of profiling floats, in *Observing the Oceans in the 21st Century*, C. J. Koblinsky and N. R. Smith, eds., GODAE Project Office, Bureau of Meteorology, Melbourne., 248-258.

Boyer, T. P., C. Stephens, J. I. Antonov, M. E. Conkright, R. A. Locarnini, T. D. O'Brien, and H. E. Garcia (2002), World Ocean Atlas 2001, vol. 2: Salinity, NOAA Atlas NESDIS 50, U.S. Gov. Print. Off., Washington, D. C., 165pp.

Gandin, L. S. (1963), Objective Analysis of the Meteorological Field, *Gidrometeorologicheskoe Izdate'stvo*, Leningrad, 286 pp.

Gill, A. E. (1982), Atmosphere-Ocean Dynamics, Elsevier, New York, 662 pp.

Hosoda, S., and S. Minato (2003), Objective analysis with Argo float and TRITON buoy data for temperature and salinity fields in the Pacific Ocean, *JAMSTECR, 48*, 67-83.

Hosoda S., S. Minato, and N. Shikama (2006), Seasonal temperature variation below the thermocline detected by Argo floats, *Geophys. Res. Lett., 33*, L13604, doi:10.1029/2006GL026070.

Meyers, G., H. Phillips, N. Smith, and J. Sprintall (1991), Space and time scales for optimal interpolation of temperature: Tropical Pacific Ocean, *Prog. Oceanogr., 28*, 189-218.

Mizuno (1995), Basin scale hydrographic analysis and optimal interpolation method, *Umi no kenkyu, 4(3)*, 187-208, in Japanese with English abstract.

Stephens, C., J. I. Antonov, T. P. Boyer, M. E. Conkright, R. A. Locarnini, T. D. O'Brien, and H. E. Garcia (2002), World Ocean Atlas 2001, vol. 1:

Temperature, NOAA Atlas NESDIS 49, U.S. Gov. Print. Off., Washington, D. C., 167 pp.

Ueki, I., K. Ando, Y. Kuroda, and K. Kutsuwada (2002), Salinity variation and its effect on dynamic height along the 156E in the Pacific warm pool, *Geophys. Res. Lett., 29(14)*, 1689, doi: 10.1029/2001GL013993.

White, W. B. (1995), Design of a global observing system for gyre-scale upper ocean temperature variability, *Prog. Oceanogr., 36*, 169-217.

Wong, A. P. S., G. C. Johnson, and W. B. Owens (2003), Delayed-mode calibration of autonomous CTD profiling float salinity data by theta-S climatology, *J. Atoms. Ocean Technol., 20*, 308-318.

Wong, A. and B. King (2005), Report on first Argo delayed-mode QC workshop. First Argo delayed-mode QC workshop, 8-13 April 2005, Scripps Institute of Oceanography, La Jolla, Calif., 27 pp.